Organic Geochemistry 142 (2020) 103983

Contents lists available at ScienceDirect

Organic Geochemistry

journal homepage: www.elsevier.com/locate/orggeochem

Global temperature calibration of the Long chain Diol Index in marine surface sediments

Marijke W. de Bar [a,*], Gabriella Weiss [a,1], Caglar Yildiz [a], Sebastiaan W. Rampen [b], Julie Lattaud [a,2], Nicole J. Bale [a], Furu Mienis [a], Geert-Jan A. Brummer [a,c], Hartmut Schulz [d], Darci Rush [a], Jung-Hyun Kim [e], Barbara Donner [f], Jochen Knies [g,h], Andreas Lückge [i], Jan-Berend W. Stuut [a,c], Jaap S. Sinninghe Damsté [a,j], Stefan Schouten [a,j,*]

[a] NIOZ Royal Netherlands Institute for Sea Research, and Utrecht University, P.O. Box 59, 1790 AB Den Burg, Texel, the Netherlands
[b] Universität Göttingen, Geoscience Center, Geobiology Group, Goldschmidtstrasse 3, 37073 Göttingen, Germany
[c] Vrije Universiteit Amsterdam, Faculty of Science, Department of Earth Sciences, De Boelelaan 1085, 1081HV Amsterdam, the Netherlands
[d] Universität Tübingen, Faculty of Science, Mikropaläontologie, Hölderlinstrasse 12, 72074 Tübingen, Germany
[e] Korea Polar Research Institute (KOPRI), 26 Songdomirae-ro, Yeonsu-gu, Incheon 21990, South Korea
[f] Universität Bremen, Center for Marine Environmental Sciences, Leobener Strasse, 28359 Bremen, Germany
[g] Geological Survey of Norway (NGU), P.O. Box 6315, 7040 Trondheim, Norway
[h] CAGE – Centre for Arctic Gas Hydrate, Environment and Climate, Department of Geosciences, UiT The Arctic University of Norway, 9037 Tromsø, Norway
[i] Federal Institute for Geosciences and Natural Resources, Stilleweg 2, 30655 Hannover, Germany
[j] Utrecht University, Faculty of Geosciences, Department of Earth Sciences, P.O. Box 80115, 3508 TC Utrecht, the Netherlands

ARTICLE INFO

Article history:
Received 25 November 2019
Received in revised form 4 February 2020
Accepted 6 February 2020
Available online 7 February 2020

Keywords:
LDI core-top calibration
Long-chain diols
SST
Freshwater
Proboscia diatoms

ABSTRACT

The Long chain Diol Index (LDI) is a relatively new organic geochemical proxy for sea surface temperature (SST), based on the abundance of the C_{30} 1,15-diol relative to the summed abundance of the C_{28} 1,13-, C_{30} 1,13- and C_{30} 1,15-diols. Here we substantially extend and re-evaluate the initial core top calibration by combining the original dataset with 172 data points derived from previously published studies and 262 newly generated data points. In total, we considered 595 globally distributed surface sediments with an enhanced geographical coverage compared to the original calibration. The relationship with SST is similar to that of the original calibration but with considerably increased scatter. The effects of freshwater input (e.g., river runoff) and long-chain diol contribution from *Proboscia* diatoms on the LDI were evaluated. Exclusion of core-tops deposited at a salinity < 32 ppt, as well as core-tops with high *Proboscia*-derived C_{28} 1,12-diol abundance, resulted in a substantial improvement of the relationship between LDI and annual mean SST. This implies that the LDI cannot be directly applied in regions with a strong freshwater influence or high C_{28} 1,12-diol abundance, limiting the applicability of the LDI. The final LDI calibration ($LDI = 0.0325 \times SST + 0.1082$; $R^2 = 0.88$; $n = 514$) is not statistically different from the original calibration of Rampen et al. (2012) (https://doi.org/10.1016/j.gca.2012.01.024), although with a larger calibration error of 3 °C. This larger calibration error results from several regions where the LDI does not seem to have a strong temperature dependence with annual mean SST, posing a limitation on the application of the LDI.

1. Introduction

The present-day release of anthropogenic greenhouse gases into the atmosphere has resulted in warming of the Earth's atmosphere and surface oceans, which is expected to continue in the coming decades (IPCC, 2014). However, the actual extent of this temperature rise and its implications for global climate is difficult to accurately predict due to the complexity of the Earth's climate system. For the prediction of future climate conditions, we typically rely on computer simulations of ocean-atmosphere circulation models,

* Corresponding authors at: NIOZ Royal Netherlands Institute for Sea Research, and Utrecht University, P.O. Box 59, 1790 AB Den Burg, Texel, the Netherlands (S. Schouten).
E-mail addresses: marijkedebar@gmail.com (M.W. de Bar), s.schouten1@uu.nl (S. Schouten).
[1] Present address: Pennsylvania State University, Jordan Road, 16563, University Park, PA, USA.
[2] Present address: ETH Zurich, Rämisstrasse 101, 8092 Zurich, Switzerland.

https://doi.org/10.1016/j.orggeochem.2020.103983
0146-6380/

which in turn rely on time-series of observational data of various climate parameters. However, instrumental records only extend back to the last century. To accurately predict climate, it is essential to study natural climate evolution on geological timescales. For this purpose, a variety of climate proxies need to be used.

One of the most important climate parameters is past sea surface temperature (SST), since oceans make up more than two thirds of the world's surface, and therefore profoundly influence (and respond to) global climate. Proxies are commonly based on measurements of either inorganic or organic remnants of organisms preserved in sediment. One of the most commonly applied inorganic paleotemperature proxies uses the stable oxygen isotopic composition ($\delta^{18}O$) of the carbonate shells of foraminifera (e.g., Emiliani, 1955; Shackleton, 1967). Also, the Mg/Ca ratio measured in a foraminiferal shell is correlated with temperature (e.g., Nürnberg et al., 1996). Organic temperature proxies, on the other hand, are generally based on lipid biomarkers, which are specific for a certain organism or a group of organisms. In paleoclimate studies there are two biomarker proxies for SST that are frequently applied. The first is the $U^{K'}_{37}$ index, based on long-chain unsaturated alkenones, detected in marine sediments world-wide, which uses the ratio of the di-unsaturated C_{37} methyl alkenones over the tri-unsaturated C_{37} methyl alkenones (Brassell et al., 1986; Prahl and Wakeham, 1987). This ratio is positively correlated with temperature, since the modern-day alkenone producers (mainly *Emiliania huxleyi* and *Gephyrocapsa oceanica*; e.g., Volkman et al., 1980, Marlowe et al., 1984; Conte et al., 1995) synthesize C_{37} alkenones, of which the degree of saturation varies with growth temperature (Brassell et al., 1986; Prahl and Wakeham, 1987). The temperature range of the proxy is between −2 °C and ca. 29 °C (Müller et al., 1998; Conte et al., 2006; Tierney and Tingley, 2018).

The second proxy, TEX_{86}, is based on the distribution of isoprenoid glycerol dialkyl glycerol tetraethers (GDGTs), produced by the archaeal phylum Thaumarchaeota (see Schouten et al., 2013 for a review). These archaea synthesize GDGTs containing 0–3 cyclopentane moieties (GDGT-0 to GDGT-3) and crenarchaeol, which contains 4 cyclopentane rings and a cyclohexane moiety (Schouten et al., 2002; Sinninghe Damsté et al., 2002). The proxy is based on the relative abundance of GDGT-1, GDGT-2 and GDGT-3 and an isomer of crenarchaeol (Schouten et al., 2002). The index is positively correlated with annual mean SST, showing an increase in the number of cyclopentane moieties with increasing temperature, and can be applied, with caution, at temperatures >30 °C. All these proxies have advantages but also recognized uncertainties, and since these uncertainties are proxy-specific, SST reconstructions are ideally based on multiple proxies. Accordingly, the development of additional proxies is desired.

Rampen et al. (2012) proposed the Long chain Diol Index (LDI), based on the fractional abundances of long-chain alkyl diols (LCDs), specifically the C_{28} and C_{30} 1,13-diols and C_{30} 1,15-diols, which contain a hydroxy group at C_1 and a hydroxy group at the C_{13} or C_{15} position, respectively:

$$\mathrm{LDI} = [\mathrm{C_{30}}1,15-\mathrm{diol}]/([\mathrm{C_{28}}1,13-\mathrm{diol} + \mathrm{C_{30}}1,13-\mathrm{diol} + \mathrm{C_{30}}1,15-\mathrm{diol}]) \quad (1)$$

The LDI, based on 161 globally distributed core-top sediments, shows a strong correlation with SST described by the following transfer function:

$$\mathrm{LDI} = 0.033 \times \mathrm{SST} + 0.095 \qquad \left(n = 161;\ \mathrm{R^2} = 0.97;\ \mathrm{RE} = 2.0\ ^{\circ}\mathrm{C}\right) \quad (2)$$

The main limitation of the LDI is the fact that the producers of the 1,13-diols and 1,15-diols in the ocean are still unknown. Cultured freshwater and marine eustigmatophyte algae produce 1,13-diols and 1,15-diols (Volkman et al., 1992, 1999; Gelin et al., 1997; Méjanelle et al., 2003; Shimokawara et al., 2010; Rampen et al., 2014b), but the LCD distributions observed in the cultures are dissimilar from the distributions observed in the marine environment. Moreover, these eustigmatophytes rarely occur in the ocean (e.g., Balzano et al., 2018). In contrast, Shimokawara et al. (2010) observed that the LCD distributions in the eustigmatophyte *Nannochloropsis* sp. (containing a dominant C_{32} 1,15-diol) were similar to that observed in sediments of Lake Baikal, suggesting that eustigmatophytes might produce LCDs in lakes. Additionally, Villanueva et al. (2014) observed similar trends for 18S rRNA gene copy numbers of (yet unknown) eustigmatophytes with LCD concentrations in an African lake, confirming eustigmatophytes as potential LCD producers in freshwater. However, Rampen et al. (2014b) tested the LDI in 62 lakes and found that the correlation with temperature was weak ($R^2 = 0.33$), which is likely because of the presence of different eustigmatophytes, each possessing different LCD distributions, implying that the applicability of the LDI may be limited to the marine environment.

Besides unknown producers, other issues with the LDI have been recognized. De Bar et al. (2016) and Lattaud et al. (2017a) observed that the LDI-derived temperatures in surface sediments near river mouths significantly deviated from satellite-derived SSTs. The diol distributions are characterized by elevated C_{32} 1,15-diol abundance, due to the freshwater input where the C_{32} 1,15 diol occurs in high abundance (Rampen et al., 2014b). Consequently, applying the LDI in marine regions with riverine input should be done with caution. Rodrigo-Gámiz et al. (2015) showed that for surface sediments and suspended particulate matter (SPM) in the subpolar region around Iceland, the LDI underestimated satellite-derived SST. Relatively high C_{28} and C_{30} 1,14-diol abundances were observed in this area, which are characteristic for *Proboscia* diatoms (Sinninghe Damsté et al., 2003; Rampen et al., 2007), although they were also identified in the estuarine species *Apedinella radians* (Rampen et al., 2011). Accordingly, the authors hypothesized that *Proboscia* diatoms (at least partially) contributed to the 1,13- and 1,15-diol production, and thereby compromised the LDI. For surface sediments in the Okhotsk Sea, also a subpolar region, the LDI correlated with SST, but this relationship was statistically different from the global calibration (Lattaud et al., 2018b). Lastly, down-core applications of the LDI have shown that the index is promising as a SST proxy but often reveals a slightly larger glacial-interglacial temperature amplitude than found for $U^{K'}_{37}$ and TEX_{86} records (Rampen et al., 2012; Lopes dos Santos et al., 2013; Rodrigo-Gámiz et al., 2014; Jonas et al., 2017; de Bar et al., 2018).

Thus, despite promising down-core applications, questions remain about the calibration of this proxy and in which environments it can be applied. Therefore, in this study we substantially extended the initial global LDI core-top calibration of Rampen et al. (2012) with literature data and newly generated data, adding 434 data points and considerably increasing global coverage. Comparison with SST and salinity allowed us to determine the main controlling factors and identify potential constraints on the applicability of the LDI.

2. Materials and methods

2.1. Surface sediments

We have combined the global core-top LCD data of Rampen et al. (2012) with other previously published LCD data and newly acquired core-top data. We re-evaluated the original LDI core-top dataset of Rampen et al. (2012), consisting of 209 measurements (black dots in Fig. 1), from which 161 LDI data points were used

in the original calibration dataset. For this dataset we quantified additional diols, in particular the C_{28} 1,12-diol. Re-integration has led to minor changes in LDI values of < 0.08. For eleven samples, we could not retrieve the original data and therefore we were not able to reintegrate the LCD peak areas (indicated in the Supplementary Table S1). Differences in contributions of the selected ions to the total ion counts (*m/z* 50–800) of saturated vs unsaturated LCDs were considered by applying correction factors as described by Rampen et al. (2009). For the dataset of Rampen et al. (2012), we applied two different correction factors to the two mass spectrometer (MS) systems on which the LCDs were analyzed (Supplementary Table S1). Additionally, we integrated some previously published LCD data (pink dots in Fig. 1), i.e., the core-top sediment data from around Iceland of Rodrigo-Gámiz et al. (2015), the Iberian margin surface sediment data of de Bar et al. (2016), the Gulf of Lion, Amazon Basin, Berau delta and Kara Sea data of Lattaud et al. (2017a), the Mozambique Channel data of Lattaud et al. (2017b), the Okhotsk Sea data of Lattaud et al. (2018a) and part of the Black Sea data of Lattaud et al. (2018b). For the published LCD data of Lattaud et al. (2017a,b), we have re-evaluated the quality of the raw data (i.e., chromatographic separation, signal-to-noise levels) and based on this we used 97 of 160 data points. We adopted the LDI data from the region around Australia (Smith et al., 2013), but did not have the original MS data and thus were not able to re-evaluate the LCD distributions. Re-evaluation of data of de Bar et al. (2016) showed that the fractional abundances of the unsaturated LCDs were not corrected for the differences in contributions of the selected ions to the total mass spectrum, which is corrected here (Supplementary Table S1). In total, the previously published data comprise 233 sediment locations. Additionally, we analyzed 105 polar fractions for long-chain diols that had been analyzed previously by Kim et al. (2008, 2010; white dots in Fig. 1) for the global TEX_{86} core-top calibration. Furthermore, we analyzed 186 new core-tops from several regions for a better spatial coverage (white dots in Fig. 1). In total, 731 surface sediment samples were considered in this study.

2.2. Lipid extraction and instrumental analysis

The 186 new surface sediments (mostly 0–1 or 0–0.5 cm) were freeze-dried and extracted with an Accelerated Solvent Extractor (ASE 200; Dionex) using a dichloromethane:methanol (DCM:MeOH) mixture (9:1; v/v) at a temperature of 100 °C and a pressure of 7–8 × 10^6 Pa. Lipid extracts were dried under nitrogen and separated into three fractions (apolar, ketone, polar) using activated (2 h at 150 °C) Al_2O_3. Separation was achieved using the eluents hexane/DCM (9:1; v/v), hexane/DCM (1:1; v/v) and DCM/MeOH (1:1; v/v), respectively (Method 2 in Supplementary Table S1). The polar fractions were silylated by the addition of pyridine and N,O-*bis*(trimethylsilyl)trifluoroacetamide (BSTFA) and heating at 60 °C for 20 min. Prior to injection, ethyl acetate was added. GC–MS analyses were done on an Agilent 7890B gas chromatograph interfaced with an Agilent 5977A mass spectrometer. Samples were injected on-column at a starting temperature of 70 °C, which was programmed to 130 °C at 20 °C min^{-1}, and a subsequent gradient of 4 °C min^{-1} to the end temperature of 320 °C, which was kept for 25 min. The GC was equipped with a fused silica column (25 m × 0.32 mm) with a CP Sil-5 coating (film thickness 0.12 μm). Helium was used as carrier gas with a constant flow of 2 ml min^{-1}, and the MS operated with an ionization energy of 70 eV. We identified the LCDs in full scan, scanning from *m/z* 50 to *m/z* 850, based on their characteristic fragmentation patterns (de Leeuw et al., 1981; Versteegh et al., 1997). Quantification of the LCDs was achieved in selected ion monitoring (SIM) mode of the characteristic fragmentation ions (i.e., *m/z* 299, 313, 327 and 341; Rampen et al., 2012). The LDI was calculated according to Rampen et al. (2012) integrating the relevant peak areas in SIM mode (Eq. (1)). For the calculation of fractional abundances, we applied a correction factor for the relative contribution of the selected fragments during SIM to the total ion counts for the saturated (16.1%) vs unsaturated (9.1%) LCDs.

Lipid extraction methods for re-analyzed polar fractions (from Kim et al., 2010) and the LCD data which we re-evaluated or adopted, are described in the original literature. We have classified these methods into five groups, indicated in the Supplementary Table S1 (Methods 1–5). Generally, these methods differ in extraction protocol, i.e. ASE, ultrasonic extraction, Bligh and Dyer, or ASE followed by saponification of the extract or in fractionation protocol, i.e. two (apolar-polar) or three fraction (apolar-ketone-polar) separation using Al_2O_3, three fraction separation using silica gel or separation of core lipids and intact polar lipids over silica gel.

2.3. Oceanographic data

The LCD data were compared with temperature, salinity and nutrient data from the World Ocean Atlas 2013 (WOA13). Annual mean, seasonal sea surface temperatures (°C; 0 m depth), temperatures for different depths, and salinity were obtained from the 0.25° grid databases (decadal averages over the period of 1955–2012; Locarnini et al., 2013; Zweng et al., 2013). Annual mean phosphate and nitrate concentrations (μmol l^{-1}) were obtained from the 1° grid WOA13 databases (Garcia et al., 2014b). In case there was no temperature data for the 0.25° grid corresponding to the core-top location, we adopted the SST value for the closest 0.25° grid. For SST, we used data within 1° distance; if not available, we did not include the data. Exceptions are thirteen Antarctic sediments for which we used seasonal SST data within 1–2° degrees because, as in these regions, SST data were generally scarcer. For salinity, we used values within 1.5° distance of the core-top location, and for phosphate and nitrate we stayed within a 3° radius. For a principal component analysis, we also obtained oxygen saturation (%), dissolved oxygen (ml l^{-1}) and silicate concentrations (μmol l^{-1}) from the World Ocean Atlas 2013 (Garcia et al., 2014a,b). The oxygen and silicate data were obtained from 1° grid databases, and only data of the grids corresponding to the core-top locations were used; i.e., in cases where data were not available, we have not used data from grids nearby.

2.4. Statistical analysis

We performed Principal Component Analysis (PCA) on the fractional abundances of the various LCDs, annual mean SST, salinity, and phosphate and nitrate concentrations, using the XLSTAT software (Addinsoft, 2020) (Fig. 3). Furthermore, PCA analysis was done on LDI, dissolved oxygen, oxygen saturation, nitrate, phosphate, silicate, salinity, SST and LDI (Supplementary Fig. S4). When an LCD was not detected, its fractional abundance was considered zero. In both PCA, data points were not plotted in cases where data for one or more of the parameters (i.e., LDI, salinity, SST, phosphate, etc.) were missing, or if the fractional abundance of one of the long-chain diols was unknown (e.g., due to co-elution). R statistical software was used for multiple linear regression analyses and for the comparison of different regression slopes by means of analysis of covariance (ANCOVA).

3. Results and discussion

We have combined several data sets to extend the core-top calibration of the LDI, as originally published by Rampen et al. (2012), to re-assess the calibration of the index, and to identify potential constraints on the proxy. We have re-evaluated the

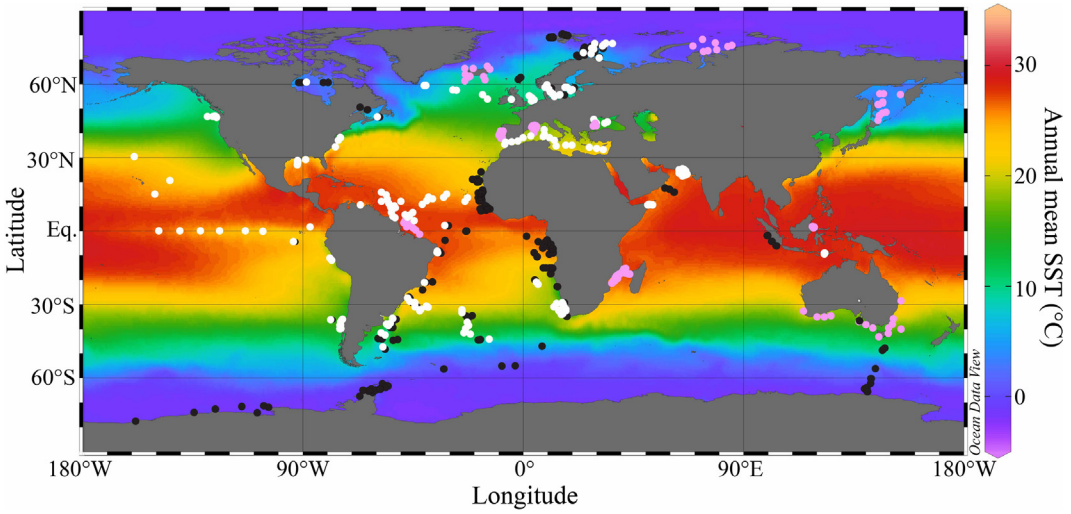

Fig. 1. Core-top sediment locations investigated in this study. Black circles indicate the surface sediments of Rampen et al. (2012), pink circles indicate surface sediments analyzed for long chain alkyl diols in previous studies (de Bar et al., 2016; Lattaud et al., 2017a,b, 2018; Smith et al., 2013; Rodrigo-Gámiz et al., 2015), and the white circles represent new surface sediment data obtained in this study. The map of sea surface temperatures (SST) is based on data of the World Ocean Atlas (2013) (Locarnini et al., 2013) and made in Ocean Data View (Schlitzer, 2015). (For interpretation of the references to colour in this figure legend, the reader is referred to the web version of this article.)

core-top data of Rampen et al. (2012), and re-evaluated and adopted previously published LCD data (Smith et al., 2013; Rodrigo-Gámiz et al., 2015; de Bar et al., 2016; Lattaud et al., 2017a,b, 2018a,b) and added new core-top data, which in total resulted in LCD distributions from 731 core-tops. Of these 731 sediment samples, we have excluded 136 samples because of quantification limit issues, related to high backgrounds obscuring the signals of the LDI-diols or low abundances of all LCDs, compromising the reliability of the LDI values. Furthermore, for certain samples fractional abundances are given but not the LDI (Supplementary Table S1), as the relative diol abundances were considered too low for index calculation. For instance, some core-tops are dominated by 1,14-diols, for which the Diol Indices were calculated, but not the LDI as the 1,13- and 1,15-diols were present in too low amounts. In total we obtained 595 LDI data points that cover an annual mean temperature range of −1.8 °C to 30.3 °C (Fig. 2; Supplementary Table S1). Although we have improved global coverage compared to Rampen et al. (2012), it must be noted that almost 40% of our surface sediments originate from the tropical temperature regime, i.e. >25 °C.

We have linearly cross-correlated our LDI core-top data with annual mean SST (WOA13; Locarnini et al., 2013), resulting in a positive regression and a coefficient of determination (R^2) of 0.82 (Fig. 2), confirming that the LDI contains a strong temperature signal. The relationship (LDI = 0.0323 × SST + 0.1111) is statistically not different from the slope and intercept (ANCOVA *p*-value > 0.1) of the original LDI-relation as proposed by Rampen et al. (2012; Eq. (2)). Additionally, we performed a PCA to reveal possible relationships between environmental factors and long-chain diol proxies (Fig. 3a) and between individual LCDs (Fig. 3b). The first component (PC) in the first PCA (Fig. 3a) explains 51.1% of the variance, with the strongest positive loadings of annual mean SST and LDI, suggesting that temperature is the main control of variance on the first component, which is confirmed by the strong correlation between the Factor 1 scores and SST, with a coefficient of determination (R^2) of 0.79 (Fig. 3c). The C_{28} and C_{30} 1,13-diols load opposite to the C_{30} 1,15-diol on Factor 1 (Fig. 3b). This is consistent with the C_{30} 1,15-diol abundance, and thus the LDI, being higher with higher SST while the 1,13-diol is more abundant with lower SST (cf. Rampen et al., 2012). Accordingly, the variance explained by Factor 1 (28%) in Fig. 3b is also likely primarily temperature, confirmed by the relatively high coefficient of determination (R^2 = 0.66) for the scores of Factor 1 and annual mean SST (Fig. 3e). The C_{32} 1,15-diol has almost no factor loading on the Factor 1 axis in both plots, suggesting that temperature has minimal influence on the abundance of the C_{32} 1,15-diol, which is consistent with the results of Rampen et al. (2012).

The fractional abundance of the C_{32} 1,15-diol (cf. de Bar et al., 2016) has a strong negative loading on the axis of Factor 2 (Fig. 3a), where salinity shows the strongest positive loading. The abundance of the C_{32} 1,15-diol has previously been linked to freshwater influence (e.g., Rampen et al., 2014a,b; de Bar et al., 2016; Lattaud et al., 2017a,b). Salinity is used as an indicator of freshwater input, suggesting the variance explained by Factor 2 is significantly influenced by freshwater input (and/or salinity), confirmed by the coefficient of determination (R^2) of 0.56 (Fig. 3d).

A number of data points do not fall close to the calibration line and lead to a decrease in coefficient of determination (R^2) from 0.97 of the original calibration of Rampen et al. (2012) to 0.82 in this study. In the following sections we will discuss factors potentially responsible for this increased scatter in the LDI calibration and evaluate possible constraints on the proxy.

3.1. Non-marine LCD contributions

Previous studies have shown that river outflow, i.e. freshwater input, can compromise the LDI (de Bar et al., 2016; Lattaud et al., 2017a), although the effect of riverine input on the LDI is likely specific for each region. For instance, de Bar et al. (2016) observed lower LDI-derived SSTs than satellite-derived SSTs in surface sediments close to the river mouths on the Portuguese margin, whereas Lattaud et al. (2017b) obtained LDI SSTs which were significantly higher than satellite SSTs for Kara Sea sediments closest to the Yenisei River. Surface sediments deposited in low salinity environments (<32 ppt), which are impacted by river inflow, are mainly derived from the Hudson Bay (salinity 26–31 ppt), the Baltic Sea (7–30 ppt), the Black Sea (11–18 ppt), and the Kara Sea (10–32 ppt). Note that the annual mean salinity at the Portuguese margin in the region studied by de Bar et al. (2016) is >32 ppt, despite the riverine input. The LDI values from the Baltic Sea, the Gulf of St.

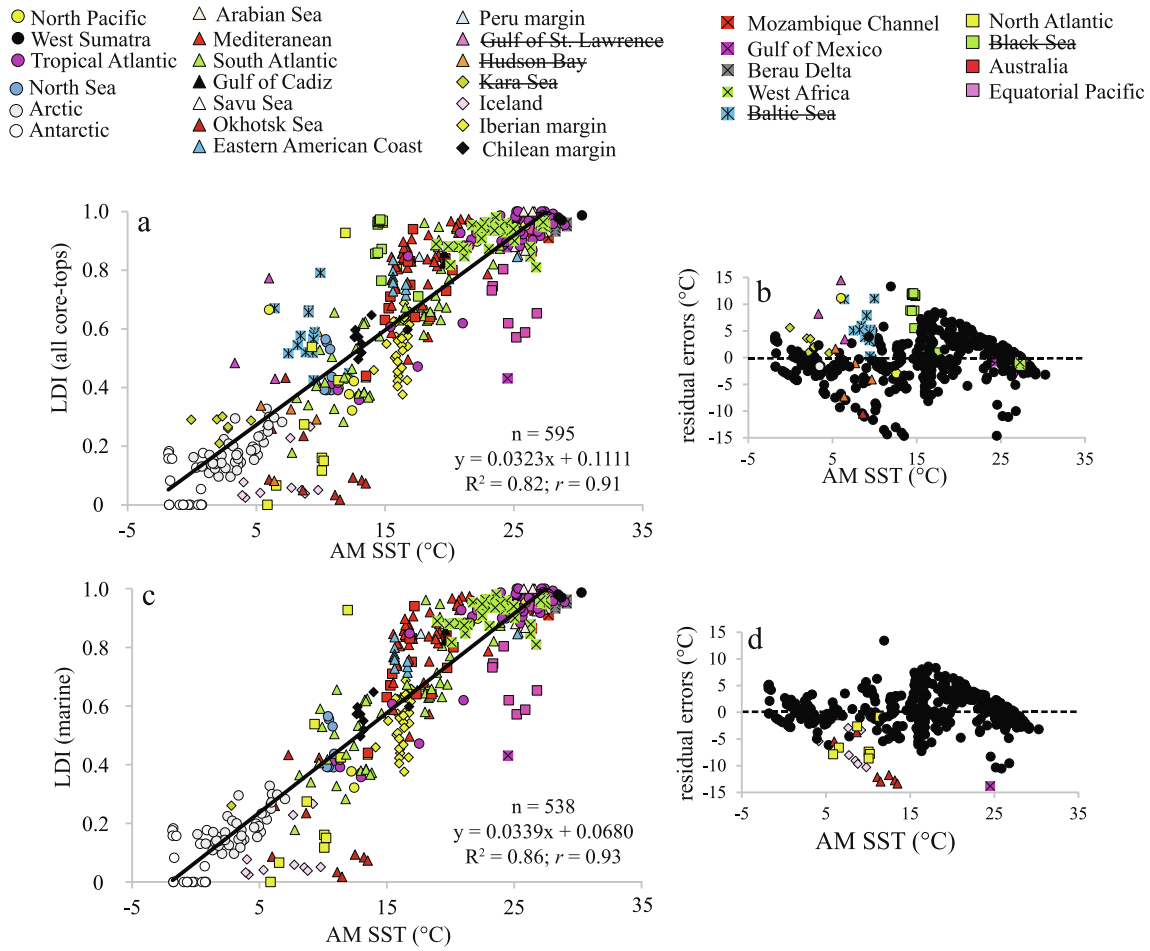

Fig. 2. (a) LDI values of all surface sediments vs annual mean SST (0 m depth; WOA13), and (c) LDI values of marine surface sediments vs annual mean SST when excluding all stations where surface salinity <32 ppt. The associated excluded sediments belong to the Hudson Bay, Black Sea, Gulf of St. Lawrence, Kara Sea (7 of 8 sediments excluded) and the Baltic Sea (indicated in the legend by strike-through). Panels (b) and (d) show the residual errors associated with the regression of (a) and (c), respectively. In panel (b), the low-salinity core-tops are highlighted which were excluded for the calibration plotted in panel (c). In panel (d), core-tops associated with *Proboscia* long-chain diol contribution are highlighted, which were excluded from the final LDI-SST calibration (Fig. 6) as discussed in Section 3.2.

Lawrence and the Black Sea are clearly positioned above the regression line (Fig. 2a) with temperature differences up to ca. + 14.5 °C. This might suggest that the LDI is unlikely to work in low salinity environments, consistent with Rampen et al. (2014b) who observed that the LDI cannot be applied to lakes. Although there is no significant relationship between salinity and the LDI or its residual error, plotting the residual errors of the LDI calibration vs salinity shows that LDI estimates for areas with the lowest salinities (Supplementary Fig. S1b) overestimate SST. Accordingly, when we exclude surface sediments deposited at salinities <32 ppt (57 samples originating from the Baltic Sea, the Black Sea, the Hudson Bay, the Gulf of St. Lawrence and the Kara Sea), the coefficient of determination improves (R^2 = 0.86; Fig. 2c). However, note that this also results in a change in calibration slope from 0.0323 to 0.0339 (Fig. 2). The core-tops from the Hudson Bay and the Gulf of St. Lawrence originate from the dataset of Rampen et al. (2012), but were also excluded in the original core-top calibration. It remains remarkable but unclear why the samples from the Portuguese margin, also influenced by freshwater but with salinities >32 ppt, do not follow this trend in overestimating SST, but provide lower SST estimates instead.

An alternative way to screen sediments for the impact of freshwater influence could be to use the abundance of the C_{32} 1,15-diol, which is often elevated near rivers (Versteegh et al., 1997, 2000; Rampen et al., 2014b; de Bar et al., 2016; Lattaud et al., 2017a,b). However, there is no clear relationship between high C_{32} 1,15-diol abundances and residual errors of the LDI (Supplementary Fig. S1a) and removal of core-tops with high C_{32} 1,15-diol abundances (i.e., >0.3), only results in a very small improvement in the coefficient of determination (R^2 = 0.83; Supplementary Fig. S1). Accordingly, the fractional abundance of the C_{32} 1,15-diol does not provide a strong indication for biases in the LDI caused by freshwater input on a global scale. We also tested if C_{32} 1,15-diol abundances can be used to correct for a possible salinity effect, by applying multiple linear regression with SST and calculated relative abundances of C_{28} and C_{30} 1,13- and C_{30} and C_{32} 1,15-diols from the original dataset. The outcome did not result in a higher coefficient of determination with SST (R^2 = 0.83), suggesting that C_{32} 1,15-diol abundances cannot be used to correct for salinity effects. In any case, this study, as well as other studies (e.g., Rampen et al., 2012; de Bar et al., 2016; Lattaud et al., 2017a), show that the application of the LDI in low salinity environments or very close to river mouths may be problematic. The weak, non-significant correlations between the LDI and its residual errors vs salinity or the fractional abundance of the C_{32} 1,15-diol indicates that neither salinity nor C_{32} 1,15-diol are conclusive indications for the compromising influence of freshwater. This influence is most likely specific for every region, and may depend, amongst others, on the freshwater sources from which long-chain diols can derive. Rivers, lakes, estuaries, inland

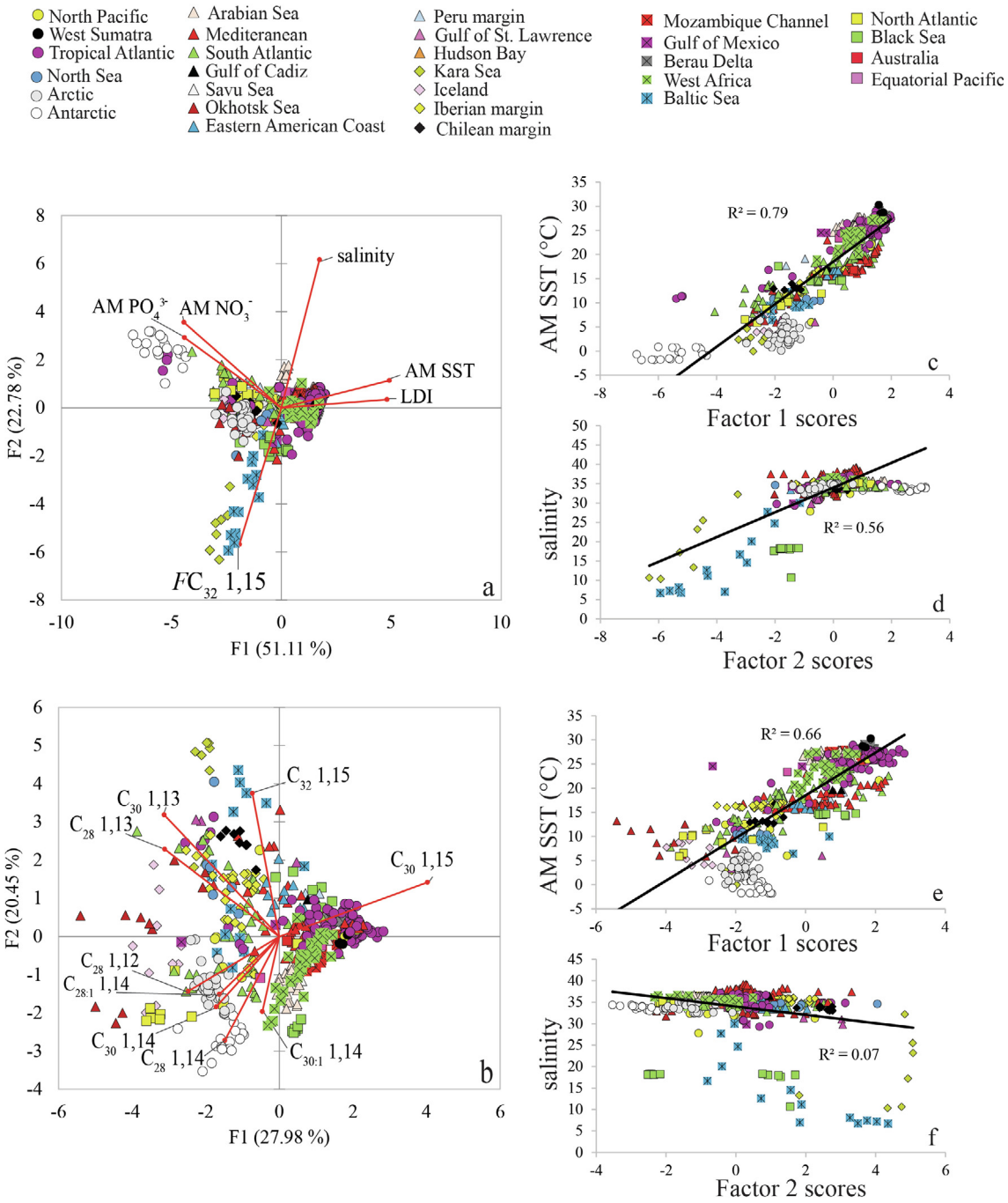

Fig. 3. (a) PCA biplot of the long-chain diol proxies, i.e., the LDI and C_{32} 1,15-diol fractional abundance, and environmental parameters, i.e., annual mean sea surface temperature (AM SST; °C), salinity, and annual mean phosphate and nitrate concentrations (μmol L^{-1}); (b) PCA biplot of the fractional abundances of the different long-chain diols. Panels (c) and (e) show the Factor 1 scores of the biplots of panels (a) and (b), respectively, correlated against annual mean SST (°C). Panels (d) and (f) show the Factor 2 scores correlated against the salinity. In cases where the fractional abundance of one or more diols was unknown for a core-top, there was no LDI value, or environmental data (World Ocean Atlas, 2013) were not available, this core-top was excluded from the PCA.

seas, wetlands, sea/land ice, etc. may each contain different diol producers, and therefore contribute different long-chain diol distributions.

3.2. Influence of Proboscia lipids on the LDI

Our dataset includes the core-top data of Rodrigo-Gámiz et al. (2015) for the subpolar region around Iceland. However, as mentioned in the introduction, the LDI substantially underestimates satellite SSTs in this region, likely because *Proboscia* diatoms seem to be at least a partial source of the 1,13-diols. Since this may also occur in other regions, we screened for the influence of *Proboscia* diatoms using two Diol Indices based on 1,14-diols vs the 1,15-diol and vs the 1,13 diols (Rampen et al., 2008; Willmott et al., 2010, respectively). Cross-correlating the temperature difference between annual mean SST and the LDI-regression based SST (from Fig. 2c) with these indices (Supplementary Fig. S2), does not reveal strong correlations, although several sediments have a high Diol Index 1 (Rampen et al., 2008) as well as a cold bias in the LDI-derived SST. However, most core-tops with such a high Diol Index

do not reveal this cold bias. Thus, the Diol Indices do not provide an unambiguous indication for a potential bias on the LDI caused by *Proboscia* LCD contribution.

We closely examined the data points which fall well below the LDI regression line, i.e., many of the Iceland data points (pink diamonds), the Okhotsk Sea (brown triangles) and the North Atlantic Ocean (yellow squares; transect Ireland-Greenland) (Fig. 2a). Examination of the chromatograms of these respective samples often showed an atypical LCD distribution compared to other marine sediments (Fig. 4). One sediment from the Gulf of Mexico also shows this unusual distribution, and interestingly this is the only data point of this region which also substantially underestimates SST when compared to the LDI regression (LDI 0.43, SST 24.5 °C; Fig. 2a). These sediments are characterized by high mono-unsaturated and saturated 1,14-diol abundances, but also relatively high C_{26} and C_{28} 1,12-diols. The Okhotsk Sea sediments also contain relatively high abundances of the C_{26} 1,13-diol. The C_{28} 1,12-diol has been observed in low amounts in lake sediments (Shimokawara et al., 2010; Rampen et al., 2014b), freshwater eustigmatophyte algae (Volkman et al., 1999; Rampen et al., 2014b) and in *Proboscia* diatoms (Rampen et al., 2007) as well as in marine sediments with high 1,14-diol concentrations (Willmott et al., 2010; Rampen et al., 2007; ten Haven and Rullkötter, 1991; de Bar et al., 2018). The C_{26} 1,12-diol has been observed in cultures of *P. inermis* and *P. indica* (Rampen et al., 2007), and in Eocene-Oligocene (between ca. 50–30 Ma) sediments from the Falkland Plateau (southwest Atlantic Ocean; Plancq et al., 2014) and the New Jersey shelf (de Bar et al., 2019). In sediments where we detected relatively high abundances of the C_{26} and C_{28} 1,12-diols, we also detected relatively high abundances of the C_{27} and C_{29} 12-hydroxy and C_{28} and C_{30} 13-hydroxy methyl alkanoates (Fig. 4). Sinninghe Damsté et al. (2003) and Rampen et al. (2007) observed C_{27} and C_{29} 12- hydroxy methyl alkanoates in cultures of *P. indica, P. alata* and *P. inermis*. Small amounts of the C_{28} and C_{30} 13-hydroxy methyl alkanoates were detected solely in *P. indica*. Since, to date, *Proboscia* is the only group of organisms known to produce these hydroxyl methyl alkanoates and 1,14- and 1,12-diols, this is a very strong indication that the LCDs and mid-chain hydroxy methyl alkanoates in these sediments are produced by *Proboscia* species. However, the unusual distributions with the high C_{26} and C_{28} 1,12-diols and C_{28} and C_{30} 12-hydroxy methyl alkanoates detected in several sediments compared to those of

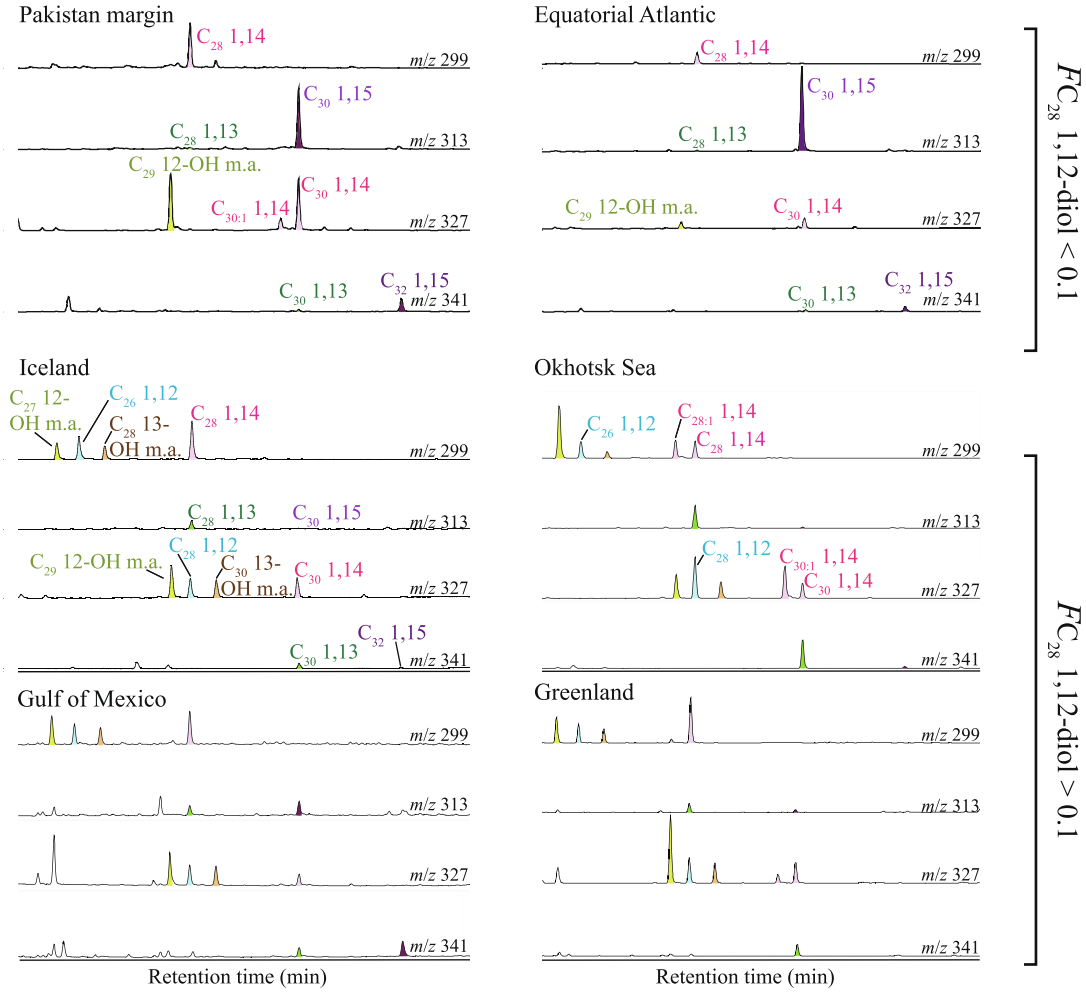

Fig. 4. Selected ion monitoring chromatograms of two sediments (two upper panels) with 'usual' long-chain diol distributions, i.e., with low 1,12-diols. The lower four panels show the chromatograms of four sediments with relatively high C_{26} and C_{28} 1,12-diols (blue), as well as the C_{27} and C_{29} 12-OH (green) and C_{28} and C_{30} 13-OH methyl alkanoates (brown). These sediments reveal LDI values which deviated substantially from the LDI calibration vs annual mean SST (see Fig. 2). The 'Greenland' sediment is classified as 'North Atlantic Ocean' in Figs. 2, 3, 5 and 6, and the "Pakistan margin" as "Arabian Sea". (For interpretation of the references to colour in this figure legend, the reader is referred to the web version of this article.)

cultures also strongly suggest that they are sourced by *Proboscia* species that have not yet been cultured and evaluated for LCDs.

The fact that the sediments with unusual distributions of 1,12-diols all reveal very low LDI values compared to the LDI regression, indicates that particular *Proboscia* species likely contribute 1,13-diols, thereby compromising the LDI. Consequently, we calculated the fractional abundance of the C_{28} 1,12-diol (with respect to the C_{28} 1,12-, 1,13-, 1,14-, C_{30} 1,13-, 1,14- and 1,15-diols):

$$FC_{28}1,12-\text{diol} = [C_{28}1,12-\text{diol}]/[C_{28}1,12 + C_{28}1,13 + C_{28}1,14 + C_{30}1,13 + C_{30}1,14 + C_{30}1,15-\text{diols}] \quad (3)$$

and subsequently plotted the FC_{28} 1,12-diol against the residual temperature errors of the LDI calibration (i.e., LDI SST – AM SST; Fig. 5). This showed that the fractional abundance of the C_{28} 1,12-diol is <0.1 for the large majority of the sediments (~95% of total), but when the fractional abundance increases, the LDI is biased towards colder temperatures (up to ca. −14 °C difference). For this reason, the relative abundance of the C_{28} 1,12-diol might serve as a better indication for the influence of certain *Proboscia* species on the LDI than the abundance of 1,14-diols. Interestingly, the regions in which we observe *Proboscia* influence on the LDI as signified by the high C_{28} 1,12-diol abundance are, except for the one core-top in the Gulf of Mexico, located between 45°N and 65 °N, suggesting that these *Proboscia* diatoms thrive mainly in these high-latitude areas. An alternative manner to correct for the influence of *Proboscia* diatoms is using multiple linear regression of SST and FC_{28} 1,12-diol. However, this did not result in an improved correlation, possibly because the relative amount of 1,13-diols produced by *Proboscia* is not a constant variable but is dependent on several environmental factors such as temperature and nutrient availability.

When we exclude core-top data with a fractional abundance of the C_{28} 1,12-diol >0.1 (24 core-tops), this improves the coefficient of determination to $R^2 = 0.88$ (Fig. 6).

The resulting LDI calibration with annual mean SST is as follows:

$$\text{LDI} = 0.0325 \times \text{SST} + 0.1082 \quad \left(n = 514;\ R^2 = 0.88;\ \text{RE} = 3.0\ ^{\circ}\text{C}\right) \quad (4)$$

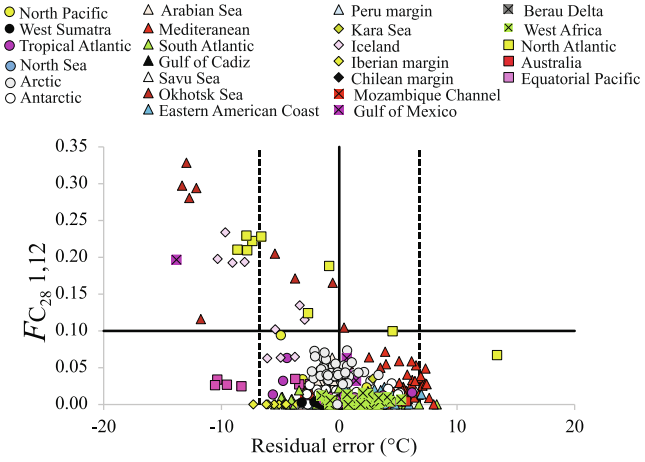

Fig. 5. The fractional abundance of the C_{28} 1,12-diol vs the residual error in SST estimation based on the regression plotted in Fig. 2c. The black solid lines indicate a fractional abundance of 0.1, and a residual error of 0. The dotted lines reflect the negative and positive 2 × SD value of 6.8 °C.

This regression equation is not statistically different from the one originally reported by Rampen et al. (2012; Eq. (2)) (ANCOVA *p*-value >0.1; although it should be noted that the data are not normally distributed).

3.3. Residual errors in estimation

Although our new correlation between LDI and annual mean SST is strong, there is also considerable scatter. Indeed, the resulting calibration error, i.e. the standard deviation on the residual errors, is 3.0 °C, which is higher than the 2.0 °C of the original calibration of Rampen et al. (2012). The residual errors of the LDI-derived SSTs (LDI SST – annual mean SST) are between −11.1 °C and 13.3 °C), without a relationship between the residuals and annual mean SST (Fig. 6b). This range of residual errors is relatively large, potentially limiting the application of the LDI as an SST proxy. Also, as can be seen in Fig. 6b, the residuals are not randomly distributed, signifying that the linear regression model does not explain all trends in the dataset. Different statistical models could be more appropriate to define the relationship between the LDI and SST, however in addition to temperature, other environmental and/or biosynthetic factors may also control the distribution of the 1,13- and 1,15-diols. LCD sources may have a seasonal occurrence, thereby registering seasonal instead of annual mean SST, and the LDI-SST relationship may be affected by regional environmental conditions such as freshwater input, nutrient conditions, and oxygen concentrations. To assess which water column parameters affect the LDI, we performed a PCA on the LDI, SST, salinity, phosphate, nitrate and silicate concentrations, dissolved oxygen, and percent oxygen saturation values from samples from the final calibration dataset (Supplementary Fig. S4). SST and the LDI show the largest factor loadings for the first PC which explains 51.8% of the total variance, indicating that temperature is the most important factor for explaining the variation in the data. Salinity loads in the same direction as SST and LDI, which may potentially be caused by the global correlation between salinity and SST. The SST and LDI factor loadings for the second PC (24.4%) are relatively low and in the same range. Hence, the PCA results provide support for the idea that SST is the most important parameter affecting the LDI.

Nevertheless, this does not exclude the possibility that in certain regions correlations between LDI and SST are absent or different. For example, it was shown for the Iberian margin that these LDI data were likely compromised by river outflow, despite a salinity >32 ppt (de Bar et al., 2016), causing a large range of LDI values despite the small range in SST. The cross-correlation of the LDI with mean seasonal SSTs reveals that the LDI correlates best with summer temperatures ($R^2 = 0.90$; Supplementary Fig. S3), also providing a more random distribution of the residuals and a more consistent calibration error over the whole temperature range. The LDI might be more reflective of seasonal temperatures rather than annual mean temperatures, depending on regional growth seasons of the source organisms which in turn depend on nutrient and upwelling conditions (e.g., Lattaud et al., 2019). In that case, an increase in scatter of the calibration is not in the LDI, but in the temperature the LDI is calibrated against.

Another issue might be that the proxy signal is not reflecting surface conditions. However, when correlating the LDI with annual mean sea temperatures from different water depths, highest coefficients of determination were observed for temperatures from the upper 30 m of the water column (R^2 = ca. 0.88), similar to Rampen et al. (2012). This is also in agreement with Balzano et al. (2018) who assessed long-chain diol concentrations for different water depths along a longitudinal transect across the tropical Atlantic, where highest concentrations were observed for the upper 20–30 m. Moreover, de Bar et al. (2019) calculated LDI temperatures

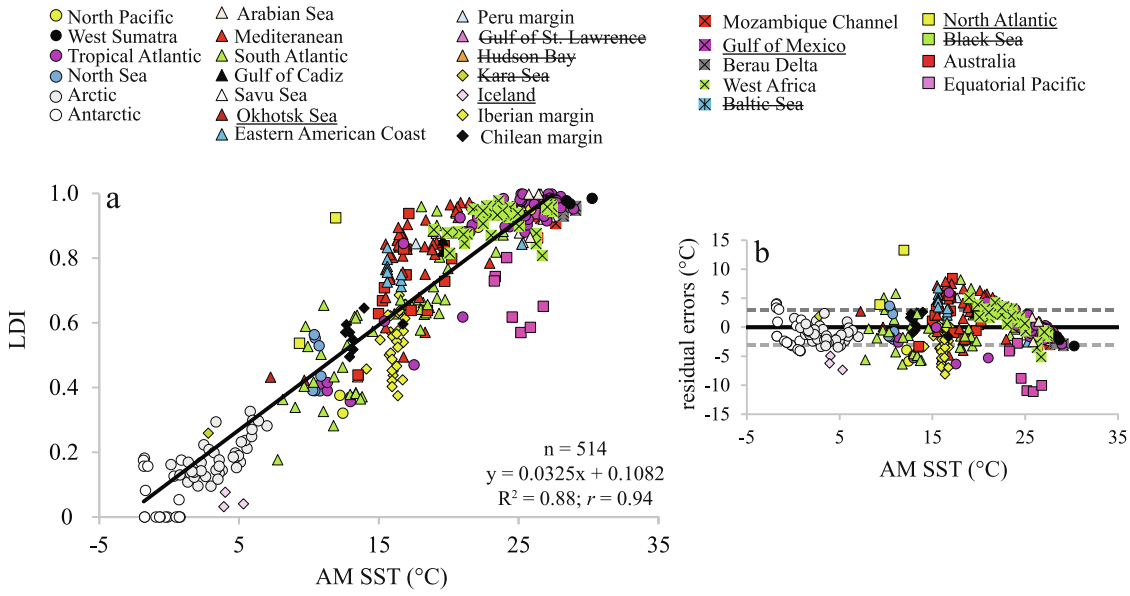

Fig. 6. (a) LDI calibration after exclusion of estuarine sediments (salinity < 32 ppt), as well as surface sediments in which the fractional abundance of the C_{28} 1,12-diol is >0.1. Regions in which surface sediments were excluded based on the C_{28} 1,12-diol abundance and salinity are indicated by underline and strike-through in the legend, respectively; (b) Residual SST errors (LDI SST – annual mean SST) against annual mean SST. The black dashed line reflects a residual error of 0 °C, and the grey dashed lines reflect the standard deviation of the residual errors, i.e., the calibration error (3.0 °C).

for sediment trap time series in the tropical Atlantic, the Mozambique Channel and the Cariaco Basin, and for all three regions the calculated (flux-weighted) LDI temperatures agreed well with mean annual surface temperatures. Thus, whereas seasonality may explain some of the scatter, there are no indications that different depth habitats play a significant role.

To further illustrate that the existence of non-random residuals can partially be explained by regional differences, the residual errors are plotted in Fig. 7 on a global map. The regions where the LDI temperatures differ more than ±2SD from the regression line are mainly derived from the Mediterranean, the Equatorial Pacific and the Iberian margin. The LDI of the surface sediments in the Mediterranean overestimate annual mean SST (up 6.6 °C) while the core-tops of the equatorial Pacific show severe underestimation (up to −11.1 °C). In the Pacific sediments, the 1,14-diols are also relatively high in abundance (30–90%), but the samples do not reveal unusual LCD distributions, i.e. a high abundance of 1,12-diols. Moreover, the PCA biplot does not show that the Equatorial Pacific or the Mediterranean data cluster as distinct groups separated from the other data (Fig. 3). The reasons for the cold and warm bias in these regions remain unknown but may be due to differences in regional conditions. For instance, in the Equatorial Pacific, the LDI temperature signal might be related to the seasonal upwelling of cold waters. If the producers of 1,13 and 1,15 LCDs mainly thrive under high-nutrient conditions induced by upwelling, or during stagnant conditions, then the LDI will reflect temperatures during these times. In general, if the source organisms bloom seasonally, then the LDI will likely reflect a seasonal, rather than annual, mean SST.

Another uncertainty is the age of the core-top material extracted. Although many sediments represent the upper 0.5 or upper 1 cm (with a few comprising the upper 2 cm), they can represent different ages, as sedimentation rates can differ significantly at different locations, resulting in different time lengths reflected by the sediment. A more careful assessment of the age represented by each surface sediment can potentially improve the calibration of the LDI.

The LDI data at the upper end of the calibration (>16 °C) showed a reduction in slope. However, application of a third order polynomial equation results only in a moderate increase in coefficient of determination to 0.90 (data not shown). Therefore, we propose to use Equation 4 as the new calibration of LDI to SST, although we realize that the linear regression model does not sufficiently explain all data and other models may be needed. More regional and time-series studies are needed to assess regional influences on the LDI, and future research should also focus on the identification of the LDI-diol producers. This could lead to a better understanding of the mechanisms behind the relationship between the LDI and temperature as well as the effect of differences in the source organisms.

3.4. Implications for LDI temperature reconstructions

Our new extended LDI calibration is statistically similar to the original calibration proposed by Rampen et al. (2012), suggesting that previous temperature reconstructions based on the LDI (e.g., Lopes dos Santos et al., 2013; Warnock et al., 2018; Jonas et al., 2017) likely do not require major adjustments. The maximum temperature difference between the previous SST calibration and the present calibration is +0.45 °C at the lower end of the calibration (LDI = 0) and −0.02 °C at the upper end (LDI = 1). However, due to the substantial increase in data points included in the calibration, the residual error increased from 2 °C to 3 °C, which is larger than that of the $U^{K'}_{37}$ (1.5 °C) and the TEX^{H}_{86} (2.5 °C). Possibly, differences between proxy values observed in sediment records may now fall within proxy errors.

Importantly, our results provide new constraints on the application of the LDI. Firstly, the LDI should not be applied in low-salinity environments and environments substantially influenced by river runoff. These types of conditions can, to some degree, be assessed for past environments using other organic proxies (e.g., BIT index, δD of alkenones, dinocyst assemblages) or inorganic proxies (e.g., mineral composition). Secondly, high abundances of the C_{26} and C_{28} 1,12-diols and C_{27} and C_{29} 12-hydroxy and C_{28} and C_{30} 13-hydroxy methyl alkanoates hint at LCD contributions from *Proboscia* spp., and we advise against using LDI data when the fractional abundance of the C_{28} 1,12-diol (vs C_{28} 1,12-, 1,13-,

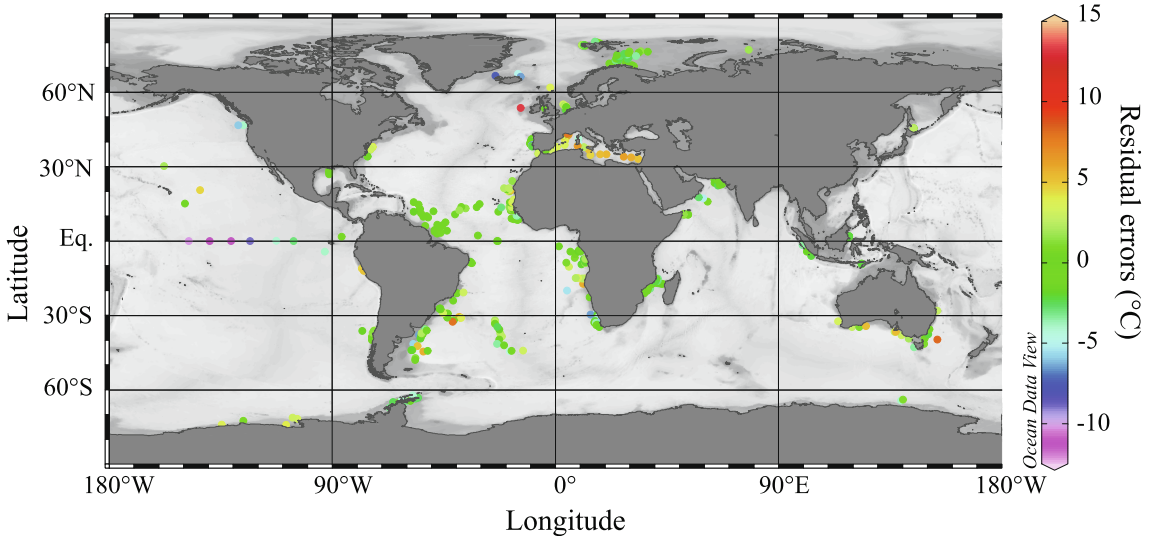

Fig. 7. Residual SST errors (LDI SST – measured annual mean SST) of the final LDI calibration plotted on the global map (created in Ocean Data View; Schlitzer, 2015).

1,14-, C_{30} 1,13-, 1,14- and 1,15-diols) is >0.1. This LCD has probably been ignored in most of the previous studies on long-chain diols, but our data show it is useful to include it in future studies to assess the potential influence of *Proboscia* LCD contribution on the LDI. Quantification of the C_{28} 1,12-diol does not require any modification of the SIM analysis method used for the standard 1,13-, 1,14- and 1,15-diols as it will be detected by the *m*/*z* 327 ion. Furthermore, caution is advised when applying the LDI in cases of high and/or variable 1,14-diol abundances (e.g., Equatorial Pacific). Since previous LDI records have not reported the abundance of C_{28} 1,12-diols we cannot evaluate whether these were compromised by *Proboscia*-derived LCDs. However, de Bar et al. (2019) calculated the LDI for the ages of ~ 11, 18, 33, 41 and 50 Ma for the Bass River core (New Jersey, USA) and observed that the LDI-derived temperatures did not agree with other paleotemperature records for this core, with LDI temperatures being between 2 and 14 °C lower as compared to the TEX_{86}^{H}-derived SSTs. Interestingly, the FC_{28} 1,12-diol varied between 0.2 and 1 for the ages of 18, 33, 41 and 50 Ma, potentially suggesting a *Proboscia* influence on the LDI at this location.

4. Conclusions

We have extended the global core-top temperature calibration of the Long chain Diol Index and confirmed that LDI values are strongly correlated with annual mean SST, but with a considerable increase in scatter and a decrease in the coefficient of determination (R^2 reduced from 0.97 to 0.82). We observed that most surface sediments from regions with low salinities, in particular sediments from the Baltic Sea and Black Sea, overestimate LDI-derived temperatures, and exclusion of these sediments (salinity < 32 ppt) improved the coefficient of determination (R^2 = 0.86). The fractional abundance of the C_{32} 1,15-diol is not a consistent indicator for freshwater influence on the LDI, since its ability to trace riverine input is likely region-specific. Examination of diol distributions with high input of 1,14-diols from *Proboscia* diatoms shows that the Diol Indices are not good indicators for identifying biases in the LDI, but that high abundances of the C_{26} and C_{28} 1,12-diols, as well as the C_{27} and C_{29} 12-hydroxy and C_{28} and C_{30} 13-hydroxy methyl alkanoates, are associated with a cold bias in the LDI-based temperatures. Therefore, we have defined a cut-off of 0.1 in the C_{28} 1,12-diol fractional abundance, which further improved the correlation between the LDI and annual mean SST. The new calibration between the LDI and SST (LDI = 0.0325 × SST + 0.1082; n = 514; R^2 = 0.88) covers a temperature range between −3.3 °C and 27.4 °C with a calibration error of 3 °C. However, the linear regression model does not sufficiently explain all of our data, due to the presence of non-random residuals in our dataset. More research is needed to constrain local and seasonal influences on the LDI, as well as to identify the source organism, in order to reduce the calibration uncertainty. The relationship is statistically similar to the Rampen et al. (2012) calibration, and thus supports previous down-core LDI applications. Our results confirm that the LDI can be used as a proxy for the reconstruction of annual mean SST in marine sediment cores, but with caveats, i.e. it should not be applied in low-salinity/freshwater influenced regions, or when the fractional abundance of the C_{28} 1,12-diol (vs C_{28} 1,12-, 1,13-, 1,14-, C_{30} 1,13-, 1,14- and 1,15-diols) is > 0.1. Accordingly, re-evaluation of the reliability of the LDI records in terms of freshwater influence (salinity, C_{32} 1,15-diol abundance) and *Proboscia* contribution (high/variable 1,14-diol abundances, C_{28} 1,12-diol abundance) is recommended. Finally, in some regions there seems to be no, or a weak relation between the LDI and annual mean SST, for reasons which are presently unclear, thereby limiting the application of the LDI.

Declaration of Competing Interest

The authors declare that they have no known competing financial interests or personal relationships that could have appeared to influence the work reported in this paper.

Acknowledgements

We thank Andy Revill, Liz Sikes, John Volkman and two anonymous reviewers for useful comments which improved the manuscript. We are grateful to various people who have worked-up or provided core-top sediments: Tjerk Veenstra, and Steven D'Hondt for Pacific core-tops recovered during the R/V *Knorr* expedition 195-3 (US National Science Foundation grant OCE-0752336), Isla Castañeda (Mozambique Channel), Ivan Tomberg and Roselyne Buscail (Gulf of Lion), Claudia Zell and David Hollander (Amazon Basin), Kees Booij (Berau Delta), Cindy de Jonge, Alina Stadnitskaia and Georgy Cherkashov (Kara Sea), Li Lo (Okhotsk Sea), Marcel van der Meer (Mediterranean), Laura Villanueva (Black Sea) and

Zeynep Erdem (Chilean margin). We thank Allert Bijleveld for statistical advice. This research has been funded by the European Research Council (ERC) under the European 555 Union's Seventh Framework Program (FP7/2007-2013) ERC grant agreement [339206] to S.S. Both S.S. and J.S.S.D. receive funding from the Netherlands Earth System Science Center (NESSC) through a Gravitation grant from the Dutch ministry for Education, Culture and Science (grant number 024.002.001).

Appendix A. Supplementary material

Supplementary data to this article can be found online at https://doi.org/10.1016/j.orggeochem.2020.103983.

Associate editor: Andrew Revill

References

Addinsoft, XLSTAT statistical and data analysis solution, Boston, USA, 2020. https://www.xlstat.com.

Balzano, S., Lattaud, J., Villanueva, L., Rampen, S.W., Brussaard, C.P.D., van Bleijswijk, J., Bale, N.J., Sinninghe Damsté, J.S., Schouten, S., 2018. A quest for the biological sources of long chain alkyl diols in the western tropical North Atlantic Ocean. Biogeosciences 15, 5951–5968.

Brassell, S.C., Eglinton, G., Marlowe, I.T., Pflaumann, U., Sarnthein, M., 1986. Molecular stratigraphy: A new tool for climatic assessment. Nature 320, 129–133.

Conte, M.H., Sicre, M.A., Rühlemann, C., Weber, J.C., Schulte, S., Schulz-Bull, D., Blanz, D., 2006. Global temperature calibration of the alkenone unsaturation index ($U^{K'}_{37}$) in surface waters and comparison with surface sediments. Geochemistry, Geophysics, Geosystems 7, 1–22.

Conte, M.H., Thompson, A., Eglinton, G., 1995. Lipid biomarker diversity in the coccolithophorid *Emiliania huxleyi* (Prymnesiophyceae) and the related species *Gephyrocapsa oceanica*. Journal of Phycology 31, 272–282.

de Bar, M.W., Dorhout, D.J.C., Hopmans, E.C., Rampen, S.W., Sinninghe Damsté, J.S., Schouten, S., 2016. Constraints on the application of long chain diol proxies in the Iberian Atlantic margin. Organic Geochemistry 101, 184–195.

de Bar, M.W., Rampen, S.W., Hopmans, E.C., Sinninghe Damsté, J.S., Schouten, S., 2019. Constraining the applicability of organic paleotemperature proxies for the last 90 Myrs. Organic Geochemistry 128, 122–136.

de Bar, M.W., Stolwijk, D.J., McManus, J.F., Sinninghe Damsté, J.S., Schouten, S., 2018. A Late Quaternary climate record based on long-chain diol proxies from the Chilean margin. Climate of the Past 14, 1783–1803.

de Leeuw, J.W., Rijpstra, W.I.C., Schenck, P.A., 1981. The occurrence and identification of C_{30}, C_{31} and C_{32} alkan-1,15-diols and alkan-15-one 1-ols in Unit I and Unit II Black Sea sediments. Geochimica et Cosmochimica Acta 45, 2281–2285.

Emiliani, C., 1955. Pleistocene temperatures. The Journal of Geology 63, 538–578.

Garcia, H.E., R.A. Locarnini, T.P. Boyer, J.I. Antonov, O.K. Baranova, M.M. Zweng, J.R. Reagan, D.R. Johnson, 2014a. World Ocean Atlas 2013, Volume 3: Dissolved Oxygen, Apparent Oxygen Utilization, and Oxygen Saturation. In: Levitus, S., Mishonov, A. (Eds.), NOAA Atlas NESDIS 75, 27 pp.

Garcia, H.E., Locarnini, R.A., Boyer, T.P., Antonov, J.I., Baranova, O.K., Zweng, M.M., Reagan, D.R., Johnson, 2014b. World Ocean Atlas 2013. Vol. 4: Dissolved Inorganic Nutrients (phosphate, nitrate, silicate). In: Levitus, S., Mishonov, A. (Eds.), NOAA Atlas NESDIS 76, 25 pp.

Gelin, F., Boogers, I., Noordeloos, A.A.M., Sinninghe Damsté, J.S., Riegman, R., de Leeuw, J.W., 1997. Resistant biomacromolecules in marine microalgae of the classes Eustigmatophyceae and Chlorophyceae: Geochemical implications. Organic Geochemistry 26, 659–675.

IPCC, 2014. Climate Change 2014: Synthesis Report. Contribution of Working Groups I, II and III to the Core Writing Team. In: Pachauri, R.K., Meyer, L.A. (Eds.), Fifth Assessment Report of the Intergovernmental Panel on Climate Change. IPCC, Geneva, Switzerland, 151 pp.

Jonas, A.S., Schwark, L., Bauersachs, T., 2017. Late Quaternary water temperature variations of the Northwest Pacific based on the lipid paleothermometers, and LDI. Deep Sea Research Part 1 Oceanographic Research Papers 125, 81–93.

Kim, J.-H., Schouten, S., Hopmans, E.C., Donner, B., Sinninghe Damsté, J.S., 2008. Global sediment core-top calibration of the TEX_{86} paleothermometer in the ocean. Geochimica et Cosmochimica Acta 72, 1154–1173.

Kim, J.-H., van der Meer, J., Schouten, S., Helmke, P., Willmott, V., Sangiorgi, F., Koç, N., Hopmans, E.C., Sinninghe Damsté, J.S., 2010. New indices and calibrations derived from the distribution of crenarchaeal isoprenoid tetraether lipids: Implications for past sea surface temperature reconstructions. Geochimica et Cosmochimica Acta 74, 4639–4654.

Lattaud, J., Kim, J.-H., de Jonge, C., Zell, C., Sinninghe Damsté, J.S., Schouten, S., 2017a. The C_{32} alkane-1,15-diol as a tracer for riverine input in coastal seas. Geochimica et Cosmochimica Acta 202, 146–158.

Lattaud, J., Dorhout, D., Schulz, H., Castañeda, I.S., Schefuß, E., Sinninghe Damsté, J.S., Schouten, S., 2017b. The C_{32} alkane-1,15-diol as a proxy of late Quaternary riverine input in coastal margins. Climate of the Past 13, 1049–1061.

Lattaud, J., Kirkels, F., Peterse, F., Freymond, C.V., Eglinton, T.I., Hefter, J., Mollenhauer, G., Balzano, S., Villanueva, L., van der Meer, M.T.J., Hopmans, E.C., Sinninghe Damsté, J.S., Schouten, S., 2018a. Long-chain diols in rivers: distribution and potential biological sources. Biogeosciences 15, 4147–4161.

Lattaud, J., Lo, L., Huang, J.-J., Chou, Y.-M., Gorbarenko, S.A., Sinninghe Damsté, J.S., Schouten, S., 2018b. A comparison of Late Quaternary organic proxy-based paleotemperature records of the Central Sea of Okhotsk. Paleoceanography and Paleoclimatology 33, 732–744.

Locarnini, R.A., Mishonov, A.V., Antonov, J.I., Boyer, T.P., Garcia, H.E., Baranova, O.K., Zweng, M.M., Paver, C.R., Reagan, J.R., Johnson, D.R., Hamilton, M., Seidov, D., 2013. World Ocean Atlas 2013, Volume 1: temperature. In: Levitus, S., Mishonov, A. (Eds.), NOAA Atlas NESDIS 73, 40 pp.

Lopes dos Santos, R.A., Spooner, M.I., Barrows, T.T., de Deckker, P., Sinninghe Damsté, J.S., Schouten, S., 2013. Comparison of organic ($U37^{K'}$, TEX86H, LDI) and faunal proxies (foraminiferal assemblages) for reconstruction of late Quaternary sea surface temperature variability from offshore southeastern Australia. Paleoceanography 28, 377–387.

Lattaud, J., Lo, L., Zeeden, C., Liu, Y.-J., Song, S.-R., van der Meer, M.T.J., Sinninghe Damsté, J.S., Schouten, S., 2019. A multiproxy study of past environmental changes in the Sea of Okhotsk during the last 1.5 Ma. Organic Geochemistry 132, 50–61.

Marlowe, I.T., Green, J.C., Neal, A.C., Brassell, S.C., Eglinton, G., Course, P.A., 1984. Long-chain (n-C_{37}–C_{39}) alkenones in the Prymnesiophyceae. Distribution of alkenones and other lipids and their taxonomic significance. British Phycological Journal 19, 203–216.

Méjanelle, L., Sanchez-Gargallo, A., Bentaleb, I., Grimalt, J.O., 2003. Long chain n-alkyl diols, hydroxy ketones and sterols in a marine eustigmatophyte, *Nannochloropsis gaditana*, and in *Brachionus plicatilis* feeding on the algae. Organic Geochemistry 34, 527–538.

Müller, P.J., Kirst, G., Ruhland, G., von Storch, I., Rosell-Melé, A., 1998. Calibration of the alkenone paleotemperature index $U^{K'}_{37}$ based on core-tops from the eastern South Atlantic and the global ocean (60°N–60°S). Geochimica et Cosmochimica Acta 62, 1757–1772.

Nürnberg, D., Bijma, J., Hemleben, C., 1996. Assessing the reliability of magnesium in foraminiferal calcite as a proxy for water mass temperatures. Geochimica et Cosmochimica Acta 60, 803–814.

Prahl, F.G., Wakeham, S.G., 1987. Calibration of unsaturation patterns in long-chain ketone compositions for palaeotemperature assessment. Nature 330, 367–369.

Rampen, S.W., Schouten, S., Wakeham, S.G., Sinninghe Damsté, J.S., 2007. Seasonal and spatial variation in the sources and fluxes of long chain diols and mid-chain hydroxy methyl alkanoates in the Arabian Sea. Organic Geochemistry 38, 165–179.

Rampen, S.W., Schouten, S., Koning, E., Brummer, G.J.A., Sinninghe Damsté, J.S., 2008. A 90 kyr upwelling record from the northwestern Indian Ocean using a novel long-chain diol index. Annual Review of Earth and Planetary Sciences 276, 207–213.

Rampen, S.W., Schouten, S., Schefuss, E., Sinninghe Damsté, J.S., 2009. Impact of temperature on long chain diol and mid-chain hydroxy methyl alkanoate composition in *Proboscia* diatoms: Results from culture and field studies. Organic Geochemistry 40, 1124–1131.

Rampen, S.W., Schouten, S., Sinninghe Damsté, J.S., 2011. Occurrence of long chain 1,14-diols in *Apedinella radians*. Organic Geochemistry 42, 572–574.

Rampen, S.W., Willmott, V., Kim, J.-H., Uliana, E., Mollenhauer, G., Schefuss, E., Sinninghe Damsté, J.S., Schouten, S., 2012. Long chain 1,13-and 1,15-diols as a potential proxy for palaeotemperature reconstruction. Geochimica et Cosmochimica Acta 84, 204–216.

Rampen, S.W., Willmott, V., Kim, J.H., Rodrigo-Gámiz, M., Uliana, E., Mollenhauer, G., Schefuss, E., Sinninghe Damsté, J.S., Schouten, S., 2014a. Evaluation of long chain 1,14-alkyl diols in marine sediments as indicators for upwelling and temperature. Organic Geochemistry 76, 39–47.

Rampen, S.W., Datema, M., Rodrigo-Gámiz, M., Schouten, S., Reichart, G.J., Sinninghe Damsté, J.S., 2014b. Sources and proxy potential of long chain alkyl diols in lacustrine environments. Geochimica et Cosmochimica Acta 144, 59–71.

Rodrigo-Gámiz, M., Martinez-Ruiz, F., Rampen, S., Schouten, S., Sinninghe Damsté, J., 2014. Sea surface temperature variations in the western Mediterranean Sea over the last 20 kyr: A dual organic proxy ($U37^{K'}$ and LDI) approach. Paleoceanography 29, 87–98.

Rodrigo-Gámiz, M., Rampen, S.W., de Haas, H., Baas, M., Schouten, S., Sinninghe Damsté, J.S., 2015. Constraints on the applicability of the organic temperature proxies $U37^{K'}$, TEX86 and LDI in the subpolar region around Iceland. Biogeosciences 12, 6573–6590.

Schlitzer, R., Ocean Data View, https://odv.awi.de, 2015.

Schouten, S., Hopmans, E.C., Sinninghe Damsté, J.S., 2013. The organic geochemistry of glycerol dialkyl glycerol tetraether lipids: A review. Organic Geochemistry 54, 19–61.

Schouten, S., Hopmans, E.C., Schefuß, E., Sinninghe Damsté, J.S., 2002. Distributional variations in marine crenarchaeotal membrane lipids: a new tool for reconstructing ancient sea water temperatures? Annual Review of Earth and Planetary Science Letters 204, 265–274.

Shackleton, N., 1967. Oxygen isotope analyses and Pleistocene temperatures re-assessed. Nature 215, 15.

Shimokawara, M., Nishimura, M., Matsuda, T., Akiyama, N., Kawai, T., 2010. Bound forms, compositional features, major sources and diagenesis of long chain, alkyl

mid-chain diols in Lake Baikal sediments over the past 28,000 years. Organic Geochemistry 41, 753–766.
Sinninghe Damsté, J.S., Rampen, S., Rijpstra, W.I.C., Abbas, B., Muyzer, G., Schouten, S., 2003. A diatomaceous origin for long-chain diols and mid-chain hydroxy methyl alkanoates widely occurring in Quaternary marine sediments: Indicators for high-nutrient conditions. Geochimica et Cosmochimica Acta 67, 1339–1348.
Sinninghe Damsté, J.S., Rijpstra, W.I.C., Hopmans, E.C., Prahl, F.G., Wakeham, S.G., Schouten, S., 2002. Distribution of membrane lipids of planktonic Crenarchaeota in the Arabian Sea. Applied and Environmental Microbiology 68, 2997–3002.
Smith, M., de Deckker, P., Rogers, J., Brocks, J., Hope, J., Schmidt, S., Lopes dos Santos, R., Schouten, S., 2013. Comparison of $U^{K'}_{37}$, TEX^{H}_{86}, and LDI temperature proxies for reconstruction of south-east Australian ocean temperatures. Organic Geochemistry 64, 94–104.
ten Haven, H.L., Rullkötter, J., 1991. Preliminary lipid analyses of sediments recovered during Leg 117 1. In: Proceedings of the Ocean Drilling Program, Scientific Results, pp. 561–569.
Tierney, J.E., Tingley, M.P., 2018. BAYSPLINE: A new calibration for the alkenone paleothermometer. Paleoceanography and Paleoclimatology 33, 281–301.
Versteegh, G.J.M., Bosch, H.J., de Leeuw, J.W., 1997. Potential palaeoenvironmental information of C_{24} to C_{36} mid-chain diols, keto-ols and mid-chain hydroxy fatty acids; a critical review. Organic Geochemistry 27, 1–13.
Versteegh, G.J.M., Jansen, J.H.F., de Leeuw, J.W., Schneider, R.R., 2000. Mid-chain diols and keto-ols in SE Atlantic sediments: A new tool for tracing past sea surface water masses? Geochimica et Cosmochimica Acta 64, 1879–1892.
Villanueva, L., Besseling, M., Rodrigo-Gámiz, M., Rampen, S.W., Verschuren, D., Sinninghe Damsté, J.S., 2014. Potential biological sources of long chain alkyl diols in a lacustrine system. Organic Geochemistry 68, 27–30.
Volkman, J.K., Barrett, S.M., Blackburn, S.I., 1999. Eustigmatophyte microalgae are potential sources of C_{29} sterols, C_{22}–C_{28} *n*-alcohols and C_{28}–C_{32} *n*-alkyl diols in freshwater environments. Organic Geochemistry 30, 307–318.
Volkman, J.K., Eglinton, G., Corner, E.D.S., Forsberg, T.E.V., 1980. Long-chain alkenes and alkenones in the marine coccolithophorid *Emiliania huxleyi*. Phytochemistry 19, 2619–2622.
Volkman, J.K., Barrett, S.M., Dunstan, G.A., Jeffrey, S.W., 1992. C_{30}–C_{32} alkyl diols and unsaturated alcohols in microalgae of the class Eustigmatophyceae. Organic Geochemistry 18, 131–138.
Warnock, J.P., Bauersachs, T., Kotthoff, U., Brandt, H.T., Andren, E., 2018. Holocene environmental history of the Angermanalven Estuary, northern Baltic Sea. Boreas 47, 593–608.
Willmott, V., Rampen, S.W., Domack, E., Canals, M., Sinninghe Damsté, J.S., Schouten, S., 2010. Holocene changes in *Proboscia* diatom productivity in shelf waters of the north-western Antarctic Peninsula. Antarctic Science 22, 3–10.
Zweng, M.M., Reagan, J.R., Antonov, J.I., Locarnini, R.A., Mishonov, A.V., Boyer, T.P., Garcia, H.E., Baranova, O.K., Johnson, D.R., Seidov, D., Biddle, M.M., 2013.World Ocean Atlas 2013, Volume 2: Salinity. In: Levitus, S., Mishonov, A. (Eds.), NOAA Atlas NESDIS 74, 39 pp.